Applied Catalysis B: Environmental 129 (2013) 491–500

Contents lists available at SciVerse ScienceDirect

Applied Catalysis B: Environmental

journal homepage: www.elsevier.com/locate/apcatb

Selective catalytic reduction of nitrogen oxides by ammonia over Co_3O_4 nanocrystals with different shapes

Bo Meng, Zongbin Zhao*, Xuzhen Wang, Jingjing Liang, Jieshan Qiu*

Carbon Research Laboratory, Liaoning Key Lab for Energy Materials and Chemical Engineering, State Key Lab of Fine Chemicals, Dalian University of Technology, Dalian 116023, China

ARTICLE INFO

Article history:
Received 8 December 2011
Received in revised form 17 August 2012
Accepted 24 September 2012
Available online 2 October 2012

Keywords:
Co_3O_4 nanorods
NO_x reduction
Catalyst morphology
Catalytic activity

ABSTRACT

In this work, single-crystalline one-dimensional Co_3O_4 nanorods with well-defined crystal planes as catalysts in the selective catalytic reduction of NO by ammonia are investigated. The Co_3O_4 nanorods synthesized by ethylene glycol-mediated precipitation at 160 °C predominantly expose {1 1 0} planes which are rich in Co^{3+} species, while the traditional Co_3O_4 nanoparticles expose the {0 0 1} and {1 1 1} planes which contain mainly Co^{2+} species. Compared with Co_3O_4 nanoparticles, Co_3O_4 nanorods show much higher NO_x conversion in NH_3-SCR reaction. TPD of various reactant gases, including NH_3, NO, NO/NH_3, NO/O_2, $NO/NH_3/O_2$, and transient experiment reveals Co_3O_4 nanorods adsorb a large amount of ammonia on their surface. Slight surface H_2 reduction significantly decreases the activity of Co_3O_4 nanocrystals, while O_2 re-oxidation partially recovers their catalytic activity, demonstrating the presence of Co^{3+} cations on the surface of Co_3O_4 nanocatalysts actually acts as the active sites in NH_3-SCR reaction. The present results indicate that novel catalyst with high activity can be designed by morphology control at nanoscale.

1. Introduction

Owing to the rapid development of synthetic technique for nanocrystals in the past decade, designing and synthesizing highly reactive catalysts with specific crystal morphology become possible [1–6]. This means that nanocrystals with perfect arrangement of surface atoms and reactive crystal planes can be achieved by means of shape-controlled synthesis. As a result, shape and crystal plane dependent catalytic activities of nanocrystals for different reactions have attracted intensive attentions in recent years [1–7]. As pioneers in this field, Spencer and et al. [7] first measured the surface structure sensitivity of the iron-catalyzed ammonia synthesis reaction using the (1 1 1), (1 0 0) and (1 1 0) crystal faces of iron at pressures approaching those used industrially (20 atmospheres), in which they demonstrated the activity ratio is 418:25:1 for the Fe(1 1 1), Fe(1 0 0) and Fe(110) planes. γ-Fe_2O_3 nanorods enclosed by the reactive {1 1 0} and {1 0 0} facets was found to be highly active and distinctively stable for the NH_3-selective catalytic reduction (SCR) reaction[1]. Similarly, CeO_2 nanorods with well-defined reactive planes ({0 0 1} and {1 1 0}) exhibit higher catalytic activity for CO oxidation than ceria nanoparticles with {1 1 1} planes [4].

As a material with typical spinel structure, Co_3O_4 has attracted intensive attention due to its wide applications in catalysis [2,5]. It has been known that the reactivity and selectivity of Co_3O_4 catalysts depend greatly upon the different arrangement manner of surface atoms and the number of dangling bonds on different crystal planes. Co_3O_4 nanosheets, nanobelts, nanocubes, mainly exposing the {1 1 2}, {0 1 1} and {0 0 1} planes, respectively, have been prepared in a control mode [5]. The catalytic activity order for methane combustion over these crystal planes follows the sequence of {1 1 2} > {0 1 1} ≫ {0 0 1}. Recently, in an outstanding work from Shen's group [2], it was demonstrated that Co_3O_4 nanorods predominantly exposing {1 1 0} planes show extremely high activity for CO oxidation at temperature as low as −77 °C even in the presence of moisture.

Up to now, the activities of nanocrystals that expose different crystal planes for simple reaction have been widely discussed [2–5]. However, little is known about nanocrystals with different shape and crystal planes in the multiple component reactions, such as the typical SCR. It is necessary to clarify the relationship between the reactivity of nanocrystals with well-defined reactive crystal planes and their structures for both fundamental science and practical technology in environmental catalysis. A number of metal oxide catalysts have been reported to be active for SCR reaction [8–25], however, few of these work focus on the influence of crystallite shape on the NH_3-SCR catalytic activity.

Metal oxide catalysts applied in NH_3-SCR reaction have been reviewed by Busca et al. [26]. Since SCR reaction is a redox process occurring with a redox or Mars–van Krevelen-type mechanism, metal oxides active in oxidation catalysis may also act as an active

* Corresponding authors. Tel.: +86 411 84986072; fax: +86 411 84986024.
E-mail addresses: zbzhao@dlut.edu.cn (Z. Zhao), jqiu@dlut.edu.cn (J. Qiu).

0926-3373/$ – see front matter © 2012 Elsevier B.V. All rights reserved.
http://dx.doi.org/10.1016/j.apcatb.2012.09.040

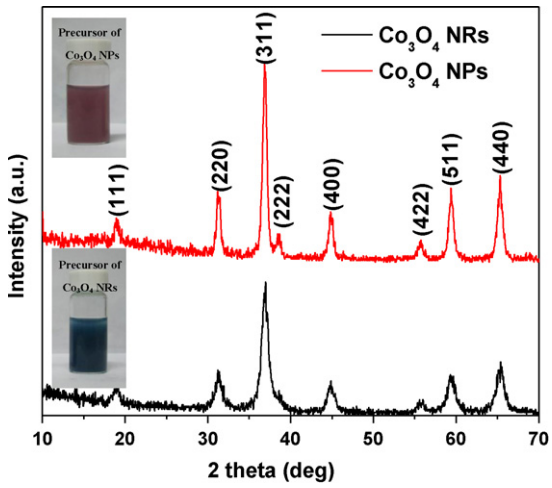

Fig. 1. XRD patterns of Co_3O_4 nanorods (NRs) and Co_3O_4 nanoparticles (NPs), insets show digital images of cobalt hydroxide carbonate prepared at 20 °C (upper inset: precursor of Co_3O_4 NPs) and 160 °C (lower inset: precursor of Co_3O_4 NRs).

component in SCR reaction. It has been reported that cobalt oxides show high catalytic activity in CO oxidation reaction [2,3,27–32] and CH_4 combustion [5,33–35], it is reasonable to deduce that they may have good activity in NH_3-SCR reaction. Cobalt oxides have been used for efficient DeNO$_x$ by catalytic reaction of NO with CO [27,36,37] or direct decomposition of NO [38–41]. In the present work, two different shapes of Co_3O_4 nanocrystals, including nanorods and nanoparticles, were synthesized and their catalytic activities in NH_3-SCR reaction were investigated. We demonstrate that the high catalytic activity of Co_3O_4 nanorods results from the Co^{3+} species distributed on Co_3O_4 nanorod surface, which facilitates the ammonia adsorption and eventually enhances their catalytic activities for NH_3-SCR reaction.

2. Experimental

2.1. Synthesis of Co_3O_4 nanorods and nanoparticles

Co_3O_4 nanorods (labeled as NRs) used in the SCR reaction were synthesized by modified ethylene glycol mediated precipitation method as reported in literature [2]. Briefly, a fixed amount of cobalt acetate tetrahydrate was dissolved in a volume of ethylene glycol and the mixture was gradually heated to 160 °C under vigorous stirring (N_2 protection) and maintained at the same temperature for 30 min. Then aqueous Na_2CO_3 (0.2 M) solution was slowly added to the mixture and blue precipitate appeared in the mixture. The final product was collected by filtration and washed with deionized water to remove any possible ionic remnants, and then dried at 60 °C overnight and calcined at 450 °C for 4 h in air.

Co_3O_4 nanoparticles (labeled as NPs) were synthesized following the same procedure and keeping the constant condition as the nanorods except using low temperature 20 °C. It should be noted that the color of the solid precipitate in the low temperature was purple rather than blue as in the case of Co_3O_4 nanorods (Fig. 1).

2.2. Catalytic activity evaluation

The NH_3-SCR reaction was performed in a continuous-flow fixed-bed quartz reactor (8 mm i.d.) under atmospheric pressure. The NH_3-SCR catalytic activity was measured as follows: 200 mg (40–60 mesh) sample was loaded into the reactor, the reactant gases (400 ppm NO, 600 ppm NH_3, 2% O_2, balanced with nitrogen) went through the reactor at a flow rate of 100 ml/min under constant temperature 75 °C. A steady state was obtained after half an hour, the concentration of NO in the outlet streams were monitored and recorded. Then the sample was heated to another fixed temperature with a ramp rate of 2.5 °C/min to get the concentration of NO at steady state. In this way, the experiment was conducted in the temperature range of 75–375 °C.

The concentrations of NO, NO_2 and O_2 in the inlet and outlet streams were monitored by an online flue gas analyzer (KM9106 Quintox, Kane International Limited) equipped with NO, NO_2 and O_2 sensors. The conversion of NO_x at a fixed temperature was calculated as follows:

$$NO_x \text{ conversion} = ([NO_x]_{in} - [NO_x]_{out})/[NO_x]_{in} \times 100\% \quad (1)$$

where $[NO_x]$ is the concentration of NO_x, namely, the sum of the NO concentration and NO_2 concentration.

2.3. NO, NH_3 adsorption and TPD

NO adsorption and temperature-programmed desorption (TPD) were measured by KM9106 Quintox online flue gas analyzer. 200 mg sample was pretreated with a 20% O_2/N_2 mixture (100 ml/min) at 450 °C for 1 h. After cooling to 20 °C, the sample was exposed to a gas mixture of 400 ppm NO in N_2 with a total flow rate of 100 ml/min until saturated adsorption. Then the sample was purged with N_2 at a flow rate of 100 ml/min for 1 h. Finally, TPD was carried out from 20 °C to 450 °C at the same flow rate of N_2 with a temperature ramp of 5 °C/min.

The procedure of gas mixture (400 ppm NO + 2% O_2, 400 ppm NO + 600 ppm NH_3, 400 ppm NO + 600 ppm NH_3 + 2% O_2) adsorption over Co_3O_4 sample was similar to NO adsorption. After gas mixture adsorption, the concentration of NO desorbed with increasing temperature was measured in real time to investigate the influence of the presence of NH_3 or/and O_2 on the adsorption behavior of NO.

The adsorption of NH_3 on the catalysts was performed at 25 °C and measured by QMS200 on-line mass spectrometer. 100 mg sample was pretreated with a 20% O_2/N_2 mixture (100 ml/min) at 450 °C for 1 h. Then the sample was exposed to a gas mixture of 10% NH_3/He at 25 °C with a flow rate of 100 ml/min until the concentration of NH_3 in the outlet was recorded constantly. After pouring with He at a flow rate of 100 ml/min for 2 h, the NH_3-TPD was recorded from 25 °C to 700 °C with a temperature ramp of 5 °C/min.

2.4. NH_3 transient response during the NH_3-SCR reaction over Co_3O_4 catalysts

The procedure for NH_3 transient response was as follows: at first, 200 mg sample was exposed to the gas mixture (400 ppm NO, 600 ppm NH_3, 2% O_2, balanced with nitrogen) with a total flow rate of 100 ml/min under constant temperature 150 °C. When the concentration of NO in the outlet streams was stable, NH_3 was removed from gas mixture and an equal volume of N_2 was added to make sure the total flow rate remain unchanged. Due to the NH_3 removal, the concentration of NO in the outlet of the reactor changed towards a new steady-state. After that, NH_3 was re-injected into the reactant gases to replace the N_2 added before, then the NO reduction in the SCR re-established a new equilibrium. The online flue gas analyzer was used to monitor the variation of NO concentration during this process.

2.5. NH_3-SCR reaction between adsorbed NH_3 and NO/O_2 gas mixture

Prior to the experiment, Co_3O_4 sample was pretreated with a 20% O_2/N_2 mixture (100 ml/min) at 450 °C for 1 h, then 200 mg sample was exposed to a gas mixture of 600 ppm NH_3 in N_2 (100 ml/min) at 150 °C until saturated adsorption (about 20 min).

Then the sample was purged with N_2 at a flow rate of 100 ml/min for 1 h. After that, the gas mixture of 400 ppm NO and 2% O_2 in N_2 was fed to the reactor at a total flow rate of 100 ml/min under constant temperature 150 °C. Co_3O_4 sample without adsorbed NH_3 was also exposed to NO/O_2 gas mixture as a comparison experiment. The concentration of NO in the outlet of the reactor was monitored by the flue gas analyzer.

2.6. Catalytic activity of Co_3O_4 nanocrystals after pre-reduction and re-oxidation

The sample (200 mg) was firstly subjected to NH_3-SCR reaction at 150 °C. Then the reaction was terminated and the used catalyst was heated to 450 °C with a temperature ramp of 5 °C/min in N_2 atmosphere to desorb the active species adsorbed on the catalyst during the reaction. After that, the catalyst was reduced by 60% H_2/N_2 mixture (100 ml/min) at different temperature (150 °C, 200 °C and 250 °C) for 20 s. Afterwards, the catalytic activities of the samples resulting from the H_2-reduction treatment at different temperature were re-tested at 150 °C. Then desorption was repeated at 450 °C (5 °C/min), and the re-oxidation to retrieve the reduced catalyst was conducted at the same temperature by exposing the sample to a 20% O_2/N_2 mixture (100 ml/min) for 1 h. Finally, the activities of the samples after oxidation for NH_3-SCR reaction were tested at 150 °C for the third time.

2.7. Materials characterization

The BET surface area was calculated from a multipoint BET analysis of the nitrogen adsorption isotherms and the N_2 adsorption–desorption isotherm was performed using a Micromeritics ASAP 2020 instrument operated at minus 196 °C. Before measurement, the sample was degassed by vacuum at 300 °C for 5 h.

The X-ray powder diffraction (XRD) patterns were recorded on a D/MAX 2400 X-ray diffractometer (Rigaku), using Cu Kα radiation operated at 40 kV and 100 mA.

The TEM and HRTEM images were obtained with a Philips Tecnai G^2 20 device operated at 180 kV. Specimens were prepared by ultrasonically suspending the sample in ethanol. A drop of the suspension was then applied onto clean holy copper grids and dried in air.

H_2 temperature-programmed reduction (H_2-TPR) was performed in a conventional set-up equipped with a thermal conductivity detector. In a typical run, 15 mg Co_3O_4 samples was used and heated to 450 °C under 5% O_2/He (10 ml/min) to remove any adsorbed species. After cooling down to 100 °C, the sample was exposed to 8% H_2/Ar (50 ml/min) and the temperature was subsequently raised from 100 °C to 600 °C with a ramp rate of 10 °C/min.

3. Results and discussion

3.1. Structures of Co_3O_4 nanocrystals

XRD analysis of Co-based catalysts has been shown in Fig. 1. The obtained diffraction reveals that the catalysts prepared at different temperature are very similar and can be perfectly indexed to the Co_3O_4 face-centered cubic structure (space group $Fd3m$(2 2 7)) with a lattice constant a = 8.065 Å, which are consistent with the values in the literature (JCPDS No. 42-1467) [5].

A typical low-magnification transmission electron microscopy (TEM) image reveals that the morphology of Co_3O_4 synthesized at 160 °C in ethylene glycol is nanorods (Fig. 2a), most of the nanorods with straight sides and regular ends, 100–300 nm in length and about 10 nm in diameter. While the morphology of Co_3O_4 synthesized at 20 °C is nanoparticles with irregular shapes and about 10–20 nm in diameter, as described in Fig. 2c.

Fig. 2b shows HRTEM images of Co_3O_4 nanorods, which reveals single crystalline structure and a respective interplanar spacing of 0.467 nm and 0.286 nm corresponding to {1 1 1} and {220} planes, respectively. The Co_3O_4 nanorod has two {0 0 1} flat planes, two {1 −1 0} side planes and two {1 1 0} end planes, mainly grows along the [110] direction and preferentially exposes the {1 1 0} planes (inset in Fig. 2b), favoring the presence of active Co^{3+} species at the surface [2,42–44]. Fig. 2d shows the HRTEM image of Co_3O_4 nanoparticles, the morphology of the nanoparticle is a truncated octahedron, surrounded by eight {1 1 1} and six {0 0 1} planes (inset in Fig. 2d), which contain mainly Co^{2+} cations at the surface [2,44].

The BET surface area of the as-prepared Co_3O_4 nanorods is 119.8 m^2/g, and that of the Co_3O_4 nanoparticles is 52.3 m^2/g. Obviously, compared with Co_3O_4 nanoparticles, Co_3O_4 nanorods expose more surface atoms.

3.2. Selective catalytic reduction of NO with NH_3 over Co_3O_4 nanorods and Co_3O_4 nanoparticles

The catalytic activities of Co_3O_4 nanorods and Co_3O_4 nanoparticles in NH_3-SCR as a function of temperature were shown in Fig. 3a. It is clear that the catalytic activity of Co_3O_4 nanorods is higher than that of nanoparticles, the maximum NO conversion over Co_3O_4 nanorods is 100% and only 65.8% over nanoparticles. However, the two catalysts start their SCR catalytic activities and achieve their maximum NO conversions at the same reaction temperature (starting and approaching maximum at 75 °C and 175 °C, respectively). After the conversion maximum, NO conversions over the two catalysts decrease when reaction temperature is above 175 °C. Intriguingly, both Co_3O_4 nanorods and Co_3O_4 nanoparticles show a second peak in their activity curves (centered at 275 °C), however, the intensity of the second peak is similar to the first one in the case of nanoparticles while only a weak shoulder peak appears in the case of nanorods. These observations make us believe different mechanism involved in the SCR with temperature over the two kinds of Co_3O_4 nanocrystals [11], furthermore, the nanorods and nanoparticles have the same catalytic active sites with difference in abundance. In other words, these Co_3O_4 nano-catalysts (nanorods and nanoparticles) have the same catalytic active species but with different surface richness, which resulted in the different reaction rates over them.

The experimental data depicted in Fig. 3b evaluate the stability of Co_3O_4 catalysts for NH_3-SCR reaction at 150 °C. Co_3O_4 nanorods show high NO_x conversion (100%) during the whole test time, while the NO_x conversion of nanoparticles decreases slightly from 39.5% to 36.1% in the first 3 h and then remain at 36.0% during the rest of the test time.

In the process of gas–solid heterogeneous catalysis, the reactant gases diffuse and adsorb onto the surface of catalyst to form surface species, final product will be given after the surface reaction and desorption [26]. Since Co_3O_4 nanorods and Co_3O_4 nanoparticles show different catalytic activity for NH_3-SCR reaction, the reaction gas adsorption capacity of two catalysts may be different. For metal oxide catalysts, there are two NH_3-SCR reaction mechanisms reported in literature [26,45], one is Eley–Rideal mechanism, involving a strongly adsorbed NH_3 and a gas-phase or weakly adsorbed NO molecules, the other is Langmuir–Hinshelwood mechanism, which involves NH_3-SCR reaction between NO and NH_3 both adsorbed on two types of catalyst active sites. These two mechanisms both demonstrate NH_3-SCR reaction involving a strongly adsorbed NH_3 on catalyst surface, therefore, it is worthy to investigate the adsorption of NH_3 on Co_3O_4 catalysts with different morphology.

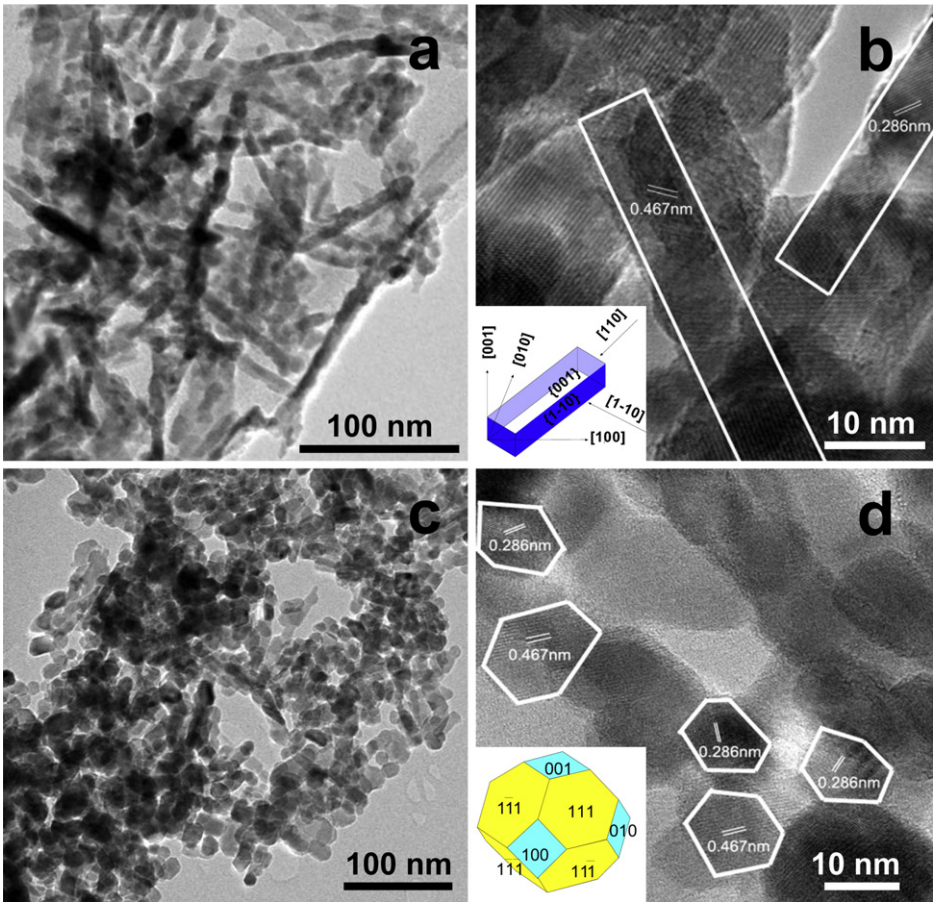

Fig. 2. (a) TEM image of Co_3O_4 NRs; (b) HRTEM image of Co_3O_4 NRs, the inset shows the schematic shape of Co_3O_4 nanorod, where blue represents the catalytically active planes; (c) TEM image of Co_3O_4 NPs; (d) HRTEM image of Co_3O_4 NPs, the inset shows the schematic shape of Co_3O_4 nanoparticle.

Fig. 4 shows NH_3-TPD profiles of Co_3O_4 nanorods and nanoparticles, Co_3O_4 nanorods desorb much more NH_3 than Co_3O_4 nanoparticles below 300 °C. The BET surface area of Co_3O_4 nanorods is 119.8 m^2/g, 2.29 times of Co_3O_4 nanoparticles, while quantitative comparison between the nanorods and nanoparticles by the integration of the desorption curves from 25 °C to 300 °C show that the adsorption capacity of the former is as much as 5.06 times of the latter at this temperature range. It can be seen clearly that the amount of NH_3 desorbed from Co_3O_4 nanoparticles is much smaller compared with that of Co_3O_4 nanorods even after excluding the impact resulting from the difference in specific surface areas. This means that there are other important reasons responsible for the high NH_3 adsorption capacity of Co_3O_4 nanorods in addition to their high surface area.

NO-TPD profiles after NO adsorption and multiple-gas co-adsorption with other reaction gases (NH_3, O_2) on Co_3O_4 nanorods are shown in Fig. 5a. When NO was adsorbed alone, the corresponding NO-TPD profile of Co_3O_4 nanorods gives rise to three distinct desorption peaks, indicating three different adsorbed N-containing species on Co_3O_4 nanorods. The three peaks, named low temperature peak, middle temperature peak, and high temperature peak, range from 50 °C to 225 °C, 225 °C to 300 °C, 300 °C

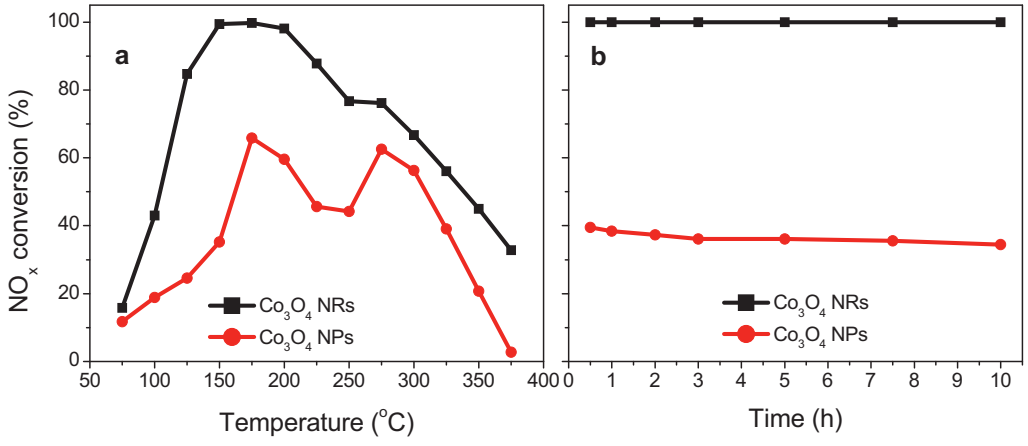

Fig. 3. NO_x conversion as a function of (a) temperature and (b) time on stream (temperature: 150 °C) over Co_3O_4 NRs and NPs.

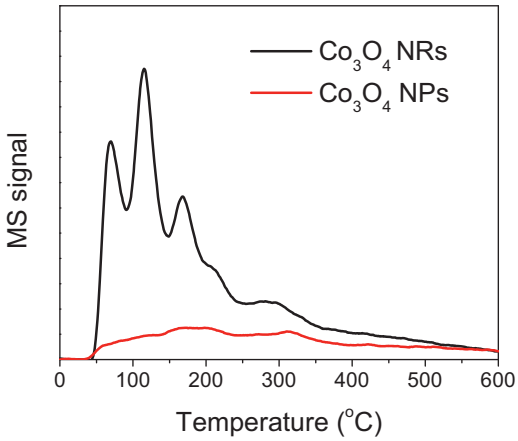

Fig. 4. TPD profiles of NH_3 after NH_3 adsorption on Co_3O_4 NRs and NPs at 25 °C.

to 400 °C, respectively. The adsorption of NO over metal oxide catalysts has also been extensively investigated in previous reports [26,46–48]. Usually, molecular NO can adsorb to form surface nitrosyls, and oxidized by oxide surfaces to give rise to nitrite ions, and nitrate ions. The thermal stability order of the adsorbed species follows the order of: nitrate ions > nitrite ions > surface nitrosyls [48]. Obviously, the NO-TPD profile in the present work is similar to the literature reported previously. The adsorption capacity of NO over nanorods can be calculated by integration from 20 °C to 450 °C, as much as 162.7 μmol/g.

In the case of NO/O_2 co-adsorption over Co_3O_4 nanorods, two desorption peaks can be observed in the corresponding NO-TPD profile. The second peak, resulting from nitrite ion desorption in the case of NO adsorption alone (ranging from 225 °C to 300 °C), disappears almost completely. One possible reason for this is that the nitrite ions have been catalytically oxidized to form nitrate ions in the presence of O_2, as shown in Fig. 5a, which can be evidenced by the fact that the high temperature desorption peak become much stronger compared with the mono-adsorption of NO. The adsorption capacity of NO from nanorods is 124.6 μmol/g in the case of co-adsorption with O_2.

When NO adsorbs together with NH_3 over nanorods, the desorption of NO from Co_3O_4 nanorods reduces greatly, calculated adsorption capacity of NO drops to 44.6 μmol/g. Obviously, the adsorption of NH_3 competes with NO on the surface of Co_3O_4 nanorods and leads to the decreasing of NO adsorption. It should be noted that the NO-TPD profile from NO/NH_3 co-adsorption appears four desorption peaks. The low temperature peak and the high temperature peak appearing in NO adsorption remain in the NO/NH_3 co-adsorption, however, the original peak in the middle temperature splits into two peaks (a shoulder peak and a separated peak).

In the multiple $NO/NH_3/O_2$ co-adsorption over nanorods, the NO-TPD profile shows three separated desorption peaks (Fig. 5a). Compared with NO mono-adsorption, the second peak shift to lower temperature region, while the first and third remain at the similar position. The adsorption capacity of NO is 78.2 μmol/g from multiple $NO/NH_3/O_2$ co-adsorption. The decreasing of NO desorption suggests a competitive adsorption between NO and NH_3, O_2. However, compared with the co-adsorption of NO/NH_3, the presence of O_2 in the multiple $NO/NH_3/O_2$ seems to enhance the adsorption of NO to some degree.

The adsorption behavior of NO over Co_3O_4 nanoparticles in the absence or presence of O_2, NH_3 has also been investigated, the resulting NO-TPD profiles are shown in Fig. 5b. The NO-TPD profile after NO adsorption on Co_3O_4 nanoparticles shows three desorption peaks, similar to the case of Co_3O_4 nanorods, indicating that NO has also three adsorbed species on Co_3O_4 nanoparticles but with relatively smaller amount. Generally, the different arrangement manner of surface atoms on Co_3O_4 nanoparticles may change the stability and amount of the NO adsorption species. According to calculating, the adsorption capacity of NO over Co_3O_4 nanoparticles is 113.4 μmol/g (nanorods 162.7 μmol/g). As for the co-adsorption of NO/O_2, the NO-TPD profile over Co_3O_4 nanoparticles also shows only two desorption peaks, similar to the case of Co_3O_4 nanorods. It seems that NO together with O_2 may form the same adsorbed species on Co_3O_4 nanorods and Co_3O_4 nanoparticles surface, with an adsorption capacity of 68.6 μmol/g on the latter (nanorods 124.6 μmol/g). In the case of NO/NH_3 co-adsorption, the amount of NO desorption from Co_3O_4 nanoparticles also decreases significantly, with an adsorption capacity of NO as low as 53.6 μmol/g. It indicates that the adsorption capacity of NH_3 on the Co_3O_4 nanoparticles surface is also much stronger than the adsorption capacity of NO. Compared with the co-adsorption of NO/NH_3, the presence of O_2 in the multiple $NO/NH_3/O_2$ system greatly promotes the adsorption of NO on Co_3O_4 nanoparticles surface (120.4 μmol/g). It should be noted that the relative intensity of the typical peaks changes with the catalyst morphology, well-defined and distinctly separated peaks from the adsorption on nanorods, while complex and irregular peaks from nanoparticles.

Based on the experimental results of NH_3 and NO adsorption and TPD (Figs. 4 and 5), obviously, Co_3O_4 nanorods can adsorb more NH_3 than Co_3O_4 nanoparticles on their surface and the adsorption capacity of NH_3 is much stronger than that of NO on both two

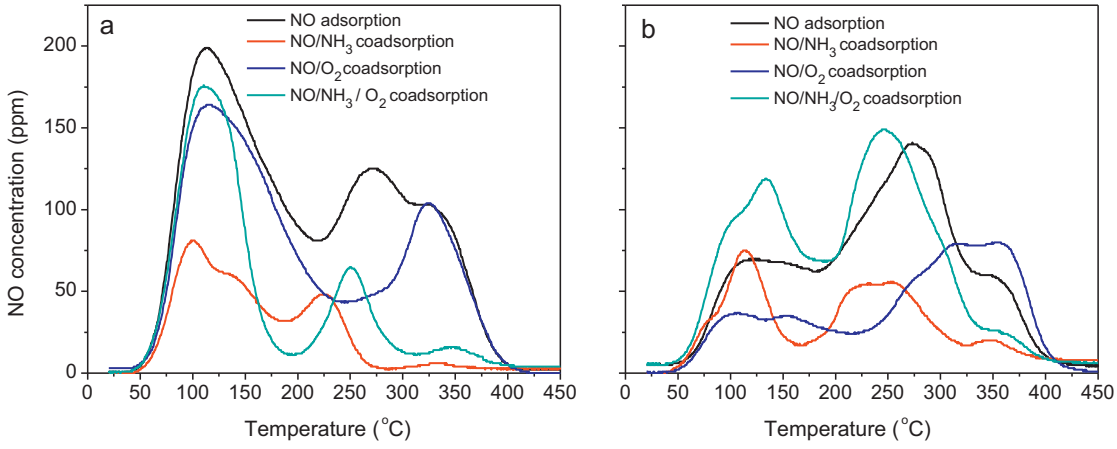

Fig. 5. TPD profiles of NO after adsorption of NO, or co-adsorption of NO/NH_3, NO/O_2, $NO/O_2/NH_3$ on (a) Co_3O_4 NRs and (b) Co_3O_4 NPs at 20 °C.

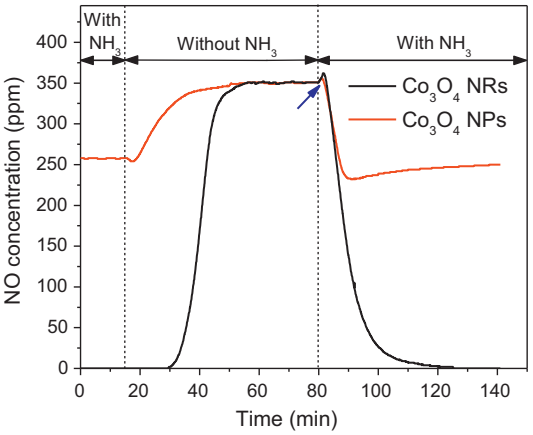

Fig. 6. NH_3 transient response during the NH_3-SCR reaction over Co_3O_4 NRs and Co_3O_4 NPs at 150 °C.

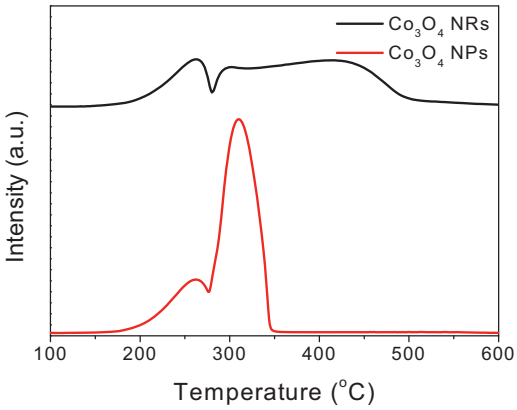

Fig. 8. H_2-TPR profiles of Co_3O_4 NRs and Co_3O_4 NPs.

catalysts. In order to further investigate the importance of NH_3 adsorption on Co_3O_4 nanorods and nanoparticles in actual NH_3-SCR reaction process, NH_3 transient response experiment has been conducted over these nanocatalysts. The corresponding experimental results over Co_3O_4 nanorods and nanoparticles were shown in Fig. 6.

When NH_3 was removed from steady reaction system, NO concentration in the outlet of the reactor should immediately increase and reach a new equilibrium theoretically due to the stopping of SCR reaction. In the case of Co_3O_4 nanoparticles, the concentration of NO in the outlet increases 2 min after NH_3 removal, while Co_3O_4 nanorods keep 100% NO conversion for about 15 min after NH_3 removal, as depicted in Fig. 6. These experimental phenomena can be explained as follows: a large amount of NH_3 has been adsorbed on Co_3O_4 nanorods surface during NH_3-SCR, NO can still react with adsorbed NH_3 after the removal of NH_3 in gas phase. In addition, the reduction of NH_3 coverage on the surface of catalyst will give more adsorption positions to NO. Since NO is simultaneously consumed by reaction and adsorption, Co_3O_4 nanorods can keep high NO conversion for a certain period of time after NH_3 removal. However, the little amount of adsorbed NH_3 on the nanoparticles can only keep a very short time for the NO reduction. Accordingly, it is reasonable to understand the appearance of NO concentration maximum (pointed by blue arrow) after the restore of NH_3 in the system, resulting from NH_3-drived desorption of NO from the Co_3O_4 nanorods surface.

To confirm the above inference, additional experiment was designed. Co_3O_4 nanocrystals were pre-adsorbed with NH_3 and then exposed to gas-phase NO and O_2 at 150 °C. The variation of NO concentrations in the outlet of the reactor during this process was shown in Fig. 7. When the gas mixture of NO and O_2 goes through the clean Co_3O_4 nanorods at 150 °C, the NO was quickly detected by gas analyzer, as described in Fig. 7a. However, when clean Co_3O_4 nanorods was pre-adsorbed with NH_3 at 150 °C, NO was detected by gas analyzer after about 8 min due to the reaction between NO and adsorbed NH_3 (Fig. 7a). The same experiment has been preformed on Co_3O_4 nanoparticles, and the results are shown in Fig. 7b. During the whole experimental time, the position of NO curve of NH_3 pre-adsorbed Co_3O_4 nanoparticles in Fig. 7b is only slightly behind the NO curve of clean Co_3O_4 nanoparticles. That means even after NH_3 pre-adsorption, there is still only a small amount of NH_3 adsorbed on Co_3O_4 nanoparticles surface and can react with NO and O_2 from the gas phase. The NH_3 pre-adsorption/reaction experiment results described in Fig. 7 further demonstrate that Co_3O_4 nanorods can adsorb much more NH_3 than Co_3O_4 nanoparticles and these adsorbed NH_3 can react with NO and O_2 on Co_3O_4 nanocrystal surface.

3.3. H_2 reduction and O_2 re-oxidation over Co_3O_4 nanocrystals for mechanism analysis

Compared with Co_3O_4 nanoparticles, Co_3O_4 nanorods exhibit higher catalytic activity and adsorb much more NH_3 in SCR as mentioned above. This indicates the close relationship between the catalytic activity of catalyst in SCR and its surface adsorption level of NH_3. In addition, the structure analysis of Co_3O_4 nanocrystals demonstrates that the Co_3O_4 nanorods predominantly expose their {1 1 0} planes, favoring the presence of Co^{3+} species at the surface,

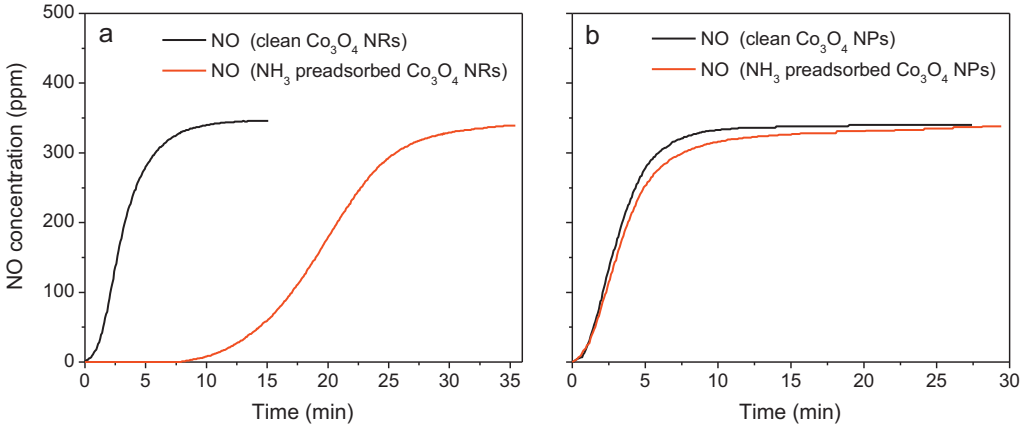

Fig. 7. NH_3-SCR reaction between adsorbed NH_3 and NO/O_2 gas mixture over NH_3 pre-adsorbed (a) Co_3O_4 NRs and (b) Co_3O_4 NPs at 150 °C.

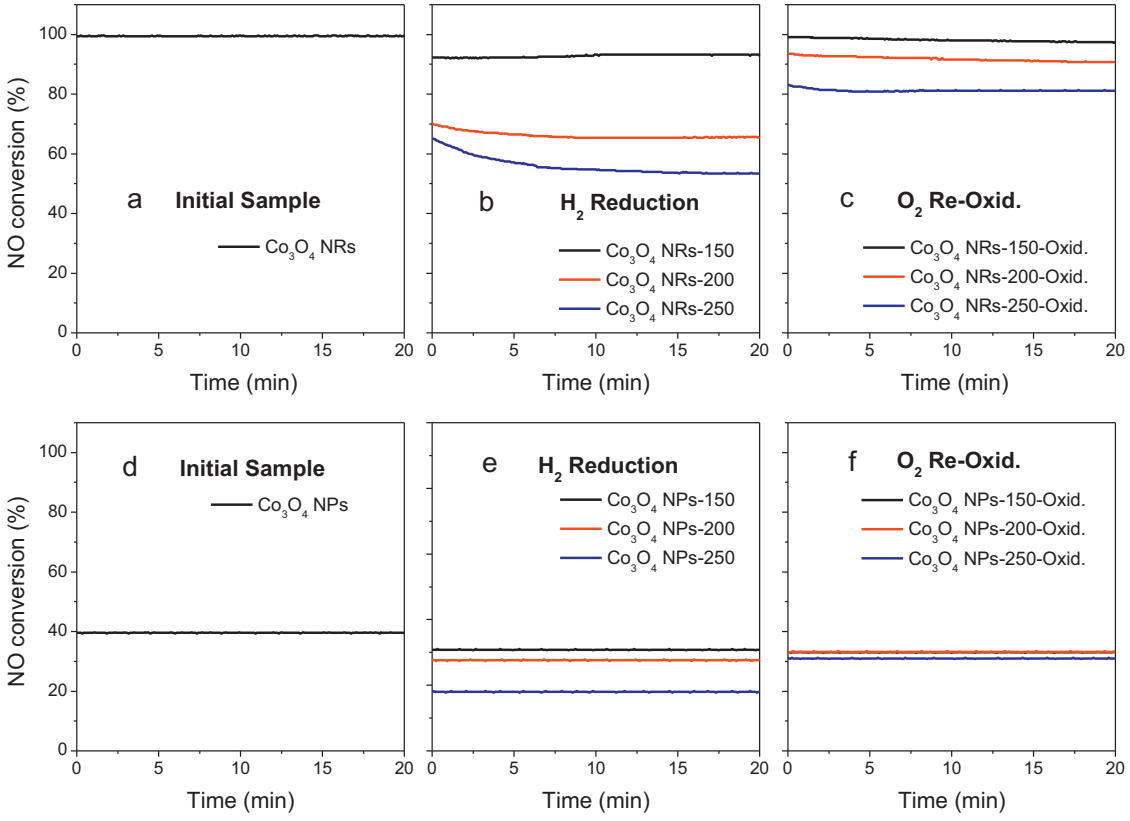

Fig. 9. Effect of H_2 reduction and O_2 re-oxidation on the catalytic activities of Co_3O_4 nanocrystals in NH_3-SCR reaction at 150 °C. (a) Initial Co_3O_4 NRs; (b) H_2-reduced Co_3O_4 NRs; (c) O_2 re-oxidized Co_3O_4 NRs; (d) initial Co_3O_4 NPs; (e) H_2-reduced Co_3O_4 NPs; (f) O_2 re-oxidized Co_3O_4 NPs.

while the Co_3O_4 nanoparticles expose the {0 0 1} and {1 1 1} planes which contain mainly Co^{2+} sites [2]. Taking into account of these factors, we believe the higher valence Co^{3+} may play critical role in the reaction. In previous work, Ramis et al. investigated the NH_3-SCR reaction mechanisms over V_2O_5/TiO_2 [49] and CuO/TiO_2 [50] with FTIR, and proposed that high valence metal ions such as V^{5+} and Cu^{2+} were first reduced by NH_3 and then re-oxidized by O_2, in which they acted as the active sites in NH_3-SCR reaction. Busca et al. [51] investigated the surface properties of cobalt oxide and found that after NH_3 adsorption at room temperature, amide NH_2 species and imide NH species can be observed on the surface of the evacuated Co_3O_4, while on the surface of the reduced Co_3O_4 (CoO), only NH_3 can be observed. Based on the above information, it is reasonable to infer that Co^{3+} cations actually act as the active sites in NH_3-SCR reaction. The abundant Co^{3+} cations on the surface of Co_3O_4 nanorods provide sufficient sites for NH_3 chemisorption and these chemisorbed NH_3 react with NO and generate N_2 and H_2O.

In order to clarify the reaction mechanism over Co_3O_4 nanocatalysts in SCR, the influence of H_2 reduction and O_2 re-oxidation on the catalytic activities was investigated. Fig. 8 shows H_2-TPR analysis of Co_3O_4 nanorods and Co_3O_4 nanoparticles. For Co_3O_4 nanorods, the reduction begins at about 150 °C, the first peak mainly below 275 °C and the second broad peak from 275 °C to 500 °C can be attributed to the reduction of Co^{3+} to Co^{2+} (step I) and Co^{2+} to Co^0 (step II), respectively. For Co_3O_4 nanoparticles, the reduction peak of step I is similar to the reduction peak of Co_3O_4 nanorods, while the reduction peak of step II becomes narrow and centers at 310 °C, meaning that it is easy for Co_3O_4 nanoparticles to be reduced to metal Co by H_2.

Based on the results of H_2-TPR, we found Co^{3+} in Co_3O_4 nanorods was reduced to Co^{2+} exclusively by H_2 reduction below 250 °C. The catalytic activities of the nanorods in SCR before and after the reduction were investigated. Prior to the H_2-reduction, the catalytic activities of samples were tested at 150 °C (Fig. 9a), it can be observed that 100% NO conversion was obtained. Then the nanorods were subjected to desorption to remove the adsorbent species on their surface (Fig. 10a). After that, the sample was exposed to 60% H_2/N_2 mixture at 150 °C, 200 °C or 250 °C about 20 s for reduction. The catalytic activities of these samples were re-tested at 150 °C (Fig. 9b). With the increasing of the reduction temperature the catalytic activity of nanorods decreased significantly. In addition, the post-reaction NO-TPD (Fig. 10b) revealed that the amount of NO desorbed from the Co_3O_4 nanorods surfaces increased with the increasing of H_2 reduction temperature. Obviously, it can be understood by taking into consideration of the competitive adsorption between NH_3 and NO. These experiment results (Figs. 9b and 10b) demonstrate that, with the increase of the reduction temperature, more and more Co^{3+} ions on the surfaces of Co_3O_4 nanorods will be reduced to Co^{2+} ions and the adsorption capacity towards NH_3 consequently decreases which ultimately reduces the catalytic activity of Co_3O_4 nanorods. In the above experiments, an extremely short time (20 s) for the H_2 reduction was used for the surface reduction to avoid the change of crystal bulk structures. Thus, after H_2 reduction, the catalytic activity for NO reduction of the catalyst can be attributed to the residual Co^{3+} species rather than Co^{2+} species on the surface of Co_3O_4 nanorods.

Re-oxidation for the recovery of catalytic activity of the nanorods was conducted with O_2 at 450 °C for 1 h after desorption. It can be surely observed the increasing of catalytic activity of nanorods in SCR after re-oxidation treatment (Fig. 9c), although the activity cannot reach as high as that before H_2 reduction. Furthermore, the catalytic activity order of these samples after re-oxidation is as same as that before oxidation, as shown in Fig. 9b. The

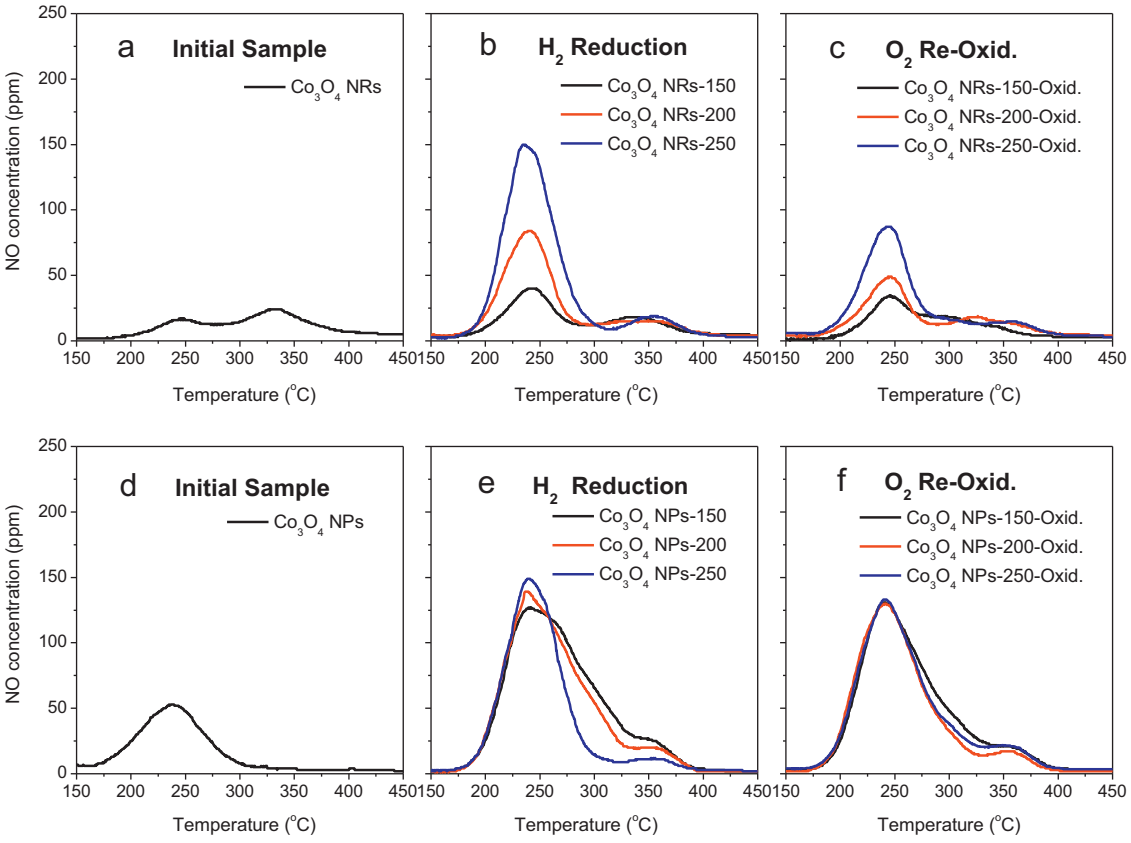

Fig. 10. TPD profiles of NO after NH_3-SCR reaction over H_2-reduced and O_2 re-oxidized Co_3O_4 nanocrystals at 150 °C. (a) Initial Co_3O_4 NRs; (b) H_2-reduced Co_3O_4 NRs; (c) O_2 re-oxidized Co_3O_4 NRs; (d) initial Co_3O_4 NPs; (e) H_2-reduced Co_3O_4 NPs; (f) O_2 re-oxidized Co_3O_4 NPs.

NO-TPD profiles over Co_3O_4 nanorods after O_2 oxidation were shown in Fig. 10c, it can be observed that the amount of NO desorbed from the sample surfaces decreased after O_2 re-oxidation. These experiments results (Figs. 9c and 10c) state clearly that after O_2 re-oxidation, partial Co^{2+} ions on Co_3O_4 nanorods surfaces can be re-oxidized to Co^{3+} ions by O_2 and the adsorption capacity of NH_3 has increased and finally promote the catalytic activity of Co_3O_4 nanorods for NH_3-SCR reaction.

The same experiments have been carried out on Co_3O_4 nanoparticles (Figs. 9d–f and 10d–f). Based on the H_2-TPR results of Co_3O_4 nanoparticles, below 250 °C, only Co^{3+} in Co_3O_4 nanoparticles can be reduced to Co^{2+} by H_2. When the nanoparticles are exposed to 60% H_2/N_2 mixture at 150 °C, 200 °C or 250 °C, with the increasing of the reduction temperature the catalytic activity of nanoparticles decreases similar to Co_3O_4 nanorods. These results suggest that Co^{3+} ions which are critical for NH_3-SCR reaction should be contained on the surface of Co_3O_4 nanopaticles, probably derived from the crystal surface defects. The post-reaction NO-TPD (Fig. 10e) reveals that the amount of NO desorbed from the Co_3O_4 nanoparticles surface increases after H_2 reduction. Owing to the Co^{3+} ions on Co_3O_4 nanoparticle surface have been reduced to Co^{2+} ions, the NH_3 adsorption capacity of Co_3O_4 nanoparticles decreases similar to Co_3O_4 nanorods, the released active sites lead to the increasing of NO adsorption.

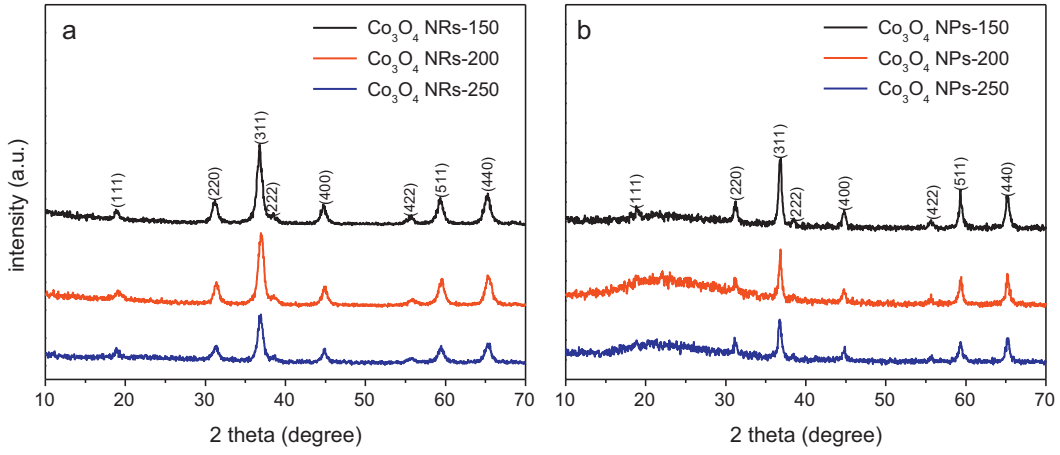

Fig. 11. XRD patterns of (a) Co_3O_4 NRs and (b) Co_3O_4 NPs after H_2 reduction at different temperature.

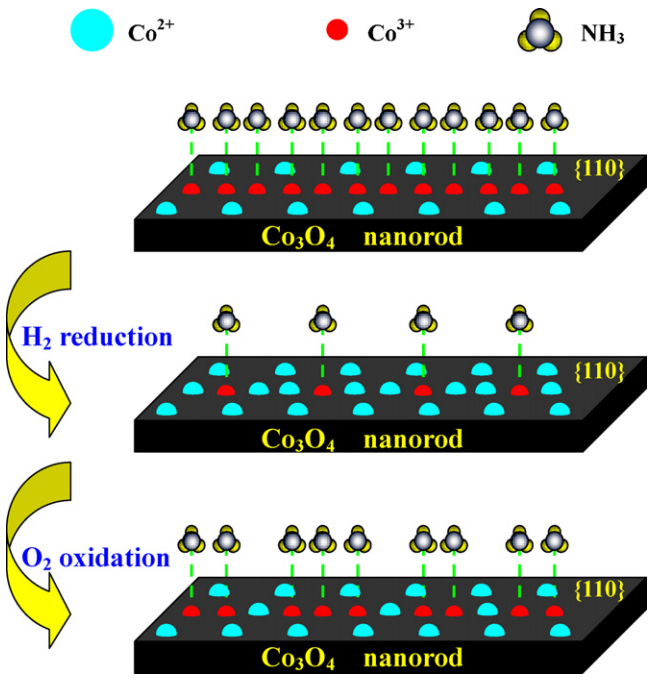

Fig. 12. Schematic illustration of the effect of H_2 and O_2 treatment on NH_3 adsorption over Co_3O_4 nanorod.

After re-oxidation, the catalytic activity of nanoparticles in SCR has been increased (as shown in Fig. 9f), although the activity cannot reach as high as that before the H_2 reduction, it also means the partial oxidation of Co^{2+} ions on Co_3O_4 nanoparticles surface like in the case of Co_3O_4 nanorods. The NO-TPD profiles over Co_3O_4 nanoparticles after O_2 oxidation are shown in Fig. 10f, it can be observed that the amount of NO desorbed from the sample surfaces decreases after O_2 re-oxidation.

Fig. 11 shows XRD patterns of reduced-Co_3O_4 nanorods and reduced-Co_3O_4 nanoparticles after H_2 reduction (20 s). All the samples in Fig. 11 are perfectly indexed to the face-centered cubic structure (space group *Fd*3*m*(2 2 7)) with a lattice constant $a = 8.065$ Å. It means that an extremely short time H_2 reduction does not change the crystal structure of Co_3O_4, the variation of the catalytic activity in SCR reaction is attributed to the reduction of Co^{3+} on the surface rather than in the bulk.

Based on the above discussion, the schematic illustration of the effect of H_2 and O_2 treatment on NH_3 adsorption over Co_3O_4 nanorods is shown in Fig. 12. Obviously, there is a direct proportion between the NH_3 adsorption capacity and the abundance of Co^{3+} on the surface of Co_3O_4 nanocatalysts. The abundant Co^{3+} ions exposed on Co_3O_4 nanorods surfaces greatly facilitate NH_3 chemisorption and finally promote the catalytic activity of Co_3O_4 nanorods for NH_3-SCR reaction. In addition, we also believe, by taking into consideration of the preparation method of the nanocrystals (from the calcination of a cobalt hydroxide carbonate precursor), there will be abundant defects on the surface of the derived Co_3O_4 nanocrystals. The presence of defects such as vacancies surely results in a locally enhanced Co^{3+} species on the surface of Co_3O_4 nanostructures. Apparently, there are much more defects on the nanorods than on nanoparticles due to the larger specific surface areas of the former. With the increasing of defects, the active sites may eventually be predominantly formed from these defects rather than from the presence of well-defined active facets. Partial restoring of the structural integrity of the catalytic materials may be accomplished by thermal annealing of the nanocrystals at high temperatures. More work is ongoing to understand the relationship between the Co_3O_4 nanostructures and their catalytic activity in SCR reaction.

4. Conclusion

Different shapes of Co_3O_4 nanocrystals were prepared and used as catalysts in SCR reaction for the removal of NO_x. Compared with Co_3O_4 nanoparticles, Co_3O_4 nanorods show significantly higher catalytic activity for NH_3-SCR reaction. The results of TPD experiments and NH_3 transient response experiment demonstrate that the adsorption capacity towards NH_3 on the surface of Co_3O_4 nanocrystals is much higher than that of NO, and Co_3O_4 nanorods can adsorb much more NH_3 than Co_3O_4 nanoparticles, which is critical for NH_3-SCR reaction. H_2 pre-reduction experiments confirm that the abundant Co^{3+} ions exposed on Co_3O_4 nanorods surfaces greatly facilitate NH_3 chemisorption and thus improve the catalytic activity of Co_3O_4 nanorods. The present results suggest that the difference in catalyst crystal morphology at nanoscale may affect the adsorption behavior of gaseous reactants on the catalyst surface and eventually enhance its catalytic activity during the reaction. Owing to the rapid development of morphology-controlled synthesis of nanostructured materials, highly reactive catalyst with specific crystal morphology can be manipulated and will play an important role in various kinds of applications such as environmental pollution control.

Acknowledgements

This work was partly supported by the National Natural Science Foundation of China (Nos. 20876026, 20836002, 21176043).

References

[1] X.L. Mou, B.S. Zhang, Y. Li, L.D. Yao, X.J. Wei, D.S. Su, W.J. Shen, Angewandte Chemie International Edition 51 (2012) 2989–2993.
[2] X.W. Xie, Y. Li, Z.Q. Li, M. Haruta, W.J. Shen, Nature 458 (2009) 746–749.
[3] X.W. Xie, W.J. Shen, Nanoscale 1 (2009) 50–60.
[4] K.B. Zhou, X. Wang, X.M. Sun, Q. Peng, Y.D. Li, Journal of Catalysis 229 (2005) 206–212.
[5] L.H. Hu, Q. Peng, Y.D. Li, Journal of the American Chemical Society 130 (2008) 16136–16137.
[6] Y. Li, Q.Y. Liu, W.J. Shen, Dalton Transactions 40 (2011) 5811–5826.
[7] N.D. Spencer, R.C. Schoonmaker, G.A. Somorjai, Journal of Catalysis 74 (1982) 129–135.
[8] N. Apostolescu, B. Geiger, K. Hizbullah, M.T. Jan, S. Kureti, D. Reichert, F. Schott, W. Weisweiler, Applied Catalysis B 62 (2006) 104–114.
[9] A.J. Shi, X.Q. Wang, T. Yu, M.Q. Shen, Applied Catalysis B 106 (2011) 359–369.
[10] M. Casapu, O. Kröcher, M. Elsener, Applied Catalysis B 88 (2009) 413–419.
[11] R. Ke, J.H. Li, X. Liang, J.M. Hao, Catalysis Communications 8 (2007) 2096–2099.
[12] M. Koebel, G. Madia, F. Raimondi, A. Wokaun, Journal of Catalysis 209 (2002) 159–165.
[13] M.F. Irfan, J.H. Goo, S.D. Kim, Applied Catalysis B 78 (2008) 267–274.
[14] J.C. Martín, P. Ávila, S. Suárez, M. Yates, A.B. Martín-Rojo, C. Barthelemy, J.A. Martín, Applied Catalysis B 67 (2006) 270–278.
[15] C.N. Costa, A.M. Efstathiou, Applied Catalysis B 72 (2007) 240–252.
[16] M. Wojciechowska, M. Zieliński, W. Przystajko, M. Pietrowski, Catalysis Today 119 (2007) 44–47.
[17] X.Y. Cuo, C. Bartholomew, W. Hecker, L.L. Baxter, Applied Catalysis B 92 (2009) 30–40.
[18] G. Busca, M.A. Larrubia, L. Arrighi, G. Ramis, Catalysis Today 107–108 (2005) 139–148.
[19] P.R. Ettireddy, N. Ettireddy, S. Mamedov, P. Boolchand, P.G. Smirniotis, Applied Catalysis B 76 (2007) 123–134.
[20] X.P. Wang, S.S. Yu, H.L. Yang, S.X. Zhang, Applied Catalysis B 71 (2007) 246–253.
[21] M. Klimczak, P. Kern, T. Heinzelmann, M. Lucas, P. Claus, Applied Catalysis B 95 (2010) 39–47.
[22] Z.P. Zhu, Z.Y. Liu, H.X. Niu, S.J. Liu, T.D. Hu, T. Liu, Y.N. Xie, Journal of Catalysis 197 (2001) 6–16.
[23] J.C. Martín, S.B. Rasmussen, S. Suárez, M. Yates, F.J. Gil-Llambías, M. Villarroel, P. Ávila, Applied Catalysis B 91 (2009) 423–427.
[24] Y. Wang, A.M. Zhu, Y.Z. Zhang, C.T. Au, X.F. Yang, C. Shi, Applied Catalysis B 81 (2008) 141–149.
[25] O. Kröcher, M. Elsener, Applied Catalysis B 77 (2008) 215–227.
[26] G. Busca, L. Lietti, G. Ramis, F. Berti, Applied Catalysis B 18 (1998) 1–36.
[27] D. Stoyanova, M. Christova, P. Dimitrova, J. Marinova, N. Kasabova, D. Panayotov, Applied Catalysis B 17 (1998) 233–244.

[28] Z.K. Zhao, X.L. Lin, R.H. Jin, Y.T. Dai, G. Wang, Catalysis Communications 12 (2011) 1448–1451.
[29] M.S. Vasilyeva, V.S. Rudnev, A.Yu. Ustinov, I.A. Korotenko, E.B. Modin, O.V. Voitenko, Applied Surface Science 257 (2010) 1239–1246.
[30] Z. Gui, J.X. Zhu, Y. Hu, Materials Chemistry and Physics 124 (2010) 243–247.
[31] I. Zacharaki, C.G. Kontoyannis, S. Boghosian, A. Lycourghiotis, C. Kordulis, Catalysis Today 143 (2009) 38–44.
[32] H.K. Lin, H.C. Chiu, H.C. Tsai, S.H. Chien, C.B. Wang, Catalysis Letters 88 (2003) 169–174.
[33] N. Bahlawane, Applied Catalysis B 67 (2006) 168–176.
[34] L.F. Liotta, G.D. Carlo, G. Pantaleo, G. Deganello, Catalysis Communications 6 (2005) 329–336.
[35] J.H. Li, X. Liang, S.C. Xu, J.M. Hao, Applied Catalysis B 90 (2009) 307–312.
[36] Z.L. Zhang, H.R. Geng, L.S. Zheng, B. Du, Journal of Alloys and Compounds 392 (2005) 317–321.
[37] L. Simonot, F. Garin, G. Maire, Applied Catalysis B 11 (1997) 181–191.
[38] M. Haneda, Y. Kintaichi, H. Hamada, Applied Catalysis B 55 (2005) 169–175.
[39] M. Haneda, Y. Kintaichi, N. Bion, H. Hamada, Applied Catalysis B 46 (2003) 473–482.
[40] P.W. Park, J.K. Kil, H.H. Kung, M.C. Kung, Catalysis Today 42 (1998) 51–60.
[41] M. Haneda, G. Tsuboi, Y. Nagao, Y. Kintaichi, H. Hamada, Catalysis Letters 97 (2004) 145–150.
[42] S.C. Petitto, M.A. Langell, Journal of Vacuum Science & Technology 22 (2004) 1690–1696.
[43] E.M. Malone, S.C. Petitto, M.A. Langell, Solid State Communications 130 (2004) 571–575.
[44] J. Ziókowski, Y. Barbaux, Journal of Molecular Catalysis 67 (1991) 199–215.
[45] H. Bosch, F. Janssen, Catalysis Today 2 (1988) 369–531.
[46] L.B. Gutierrez, E.E. Miró, M.A. Ulla, Applied Catalysis A 321 (2007) 7–16.
[47] N. Li, A.Q. Wang, M.Y. Zheng, X.D. Wang, R.H. Cheng, T. Zhang, Journal of Catalysis 225 (2004) 307–315.
[48] W.S. Kijlstra, D.S. Brands, E.K. Poels, A. Bliek, Journal of Catalysis 171 (1997) 208–218.
[49] G. Ramis, G. Busca, F. Bregani, P. Forzatti, Applied Catalysis 64 (1990) 259–278.
[50] G. Ramis, L. Yi, G. Busca, M. Turco, E. Kotur, R.J. Willey, Journal of Catalysis 157 (1995) 523–535.
[51] G. Busca, R. Guidetti, V. Lorenzelli, Journal of the Chemical Society, Faraday Transactions 86 (1990) 989–994.